Renewable Energy 251 (2025) 123308

Contents lists available at ScienceDirect

Renewable Energy

journal homepage: www.elsevier.com/locate/renene

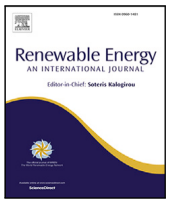

Experimental performance comparison of Ducted and Freestream hydrokinetic turbines

Kartik Naik [a,1], Marco Mangano [b,1], Bradford G. Knight [c,1], Sabet Seraj [b], Yingqian Liao [b], Jeongbin Park [a], Yulin Pan [a], Joaquim R.R.A. Martins [b], Kevin J. Maki [a], Jing Sun [a,*]

[a] University of Michigan, Naval Architecture and Marine Engineering Department, 2600 Draper Dr, Ann Arbor, MI 48109, USA
[b] University of Michigan, Aerospace Engineering Department, 1320 Beal Ave, Ann Arbor, MI 48109, USA
[c] University of Rhode Island, Ocean Engineering Department, 15 Receiving Rd, Narragansett, 02882, USA

ARTICLE INFO

Keywords:
Marine energy
Hydrokinetic turbine
Experimental characterization
Performance analysis

ABSTRACT

Hydrokinetic energy's high energy density and predictable nature make it an effective and reliable renewable resource. Ducted hydrokinetic turbines (HKT) offer benefits such as improved flow conditioning and higher power efficiency for the same reference area compared to an equivalent conventional freestream turbine. We designed and constructed an HKT system to characterize the performance of freestream and ducted turbines at various speeds and blade pitch angles in a state-of-the-art tow tank. When comparing the respective optimal blade pitch settings, the ducted turbine's power efficiency is 19% higher than that of the freestream one. Our ducted turbine measured a peak power coefficient of $C_P = 0.47$ despite unfavorable Reynolds number effects. This system's power and thrust characterization indicates that ducted turbines, with an improved design and more favorable operating conditions, would likely exceed the measured $C_P = 0.47$, laying the ground for further design optimization studies.

1. Introduction

The diversification of the renewable energy harvesting portfolio is a crucial step toward achieving global decarbonization goals while meeting the increasing demand for energy. Marine hydrokinetic (MHK) energy can play a vital part of this diversified portfolio due to its high harvesting potential and reliability. The MHK harvesting potential in the US alone is 368 TWh/year [1], which includes riverine (99 TWh/year), ocean current (49 TWh/year), and tidal (220 TWh/year) resources. These resources are more reliable and predictable than wind and solar energy. The full extent of their potential is an active field or research.

Horizontal axis turbines are the preferred choice for harvesting tidal and riverine energy [2] due to the vast engineering and operational expertise that can be transferred from the wind energy field. Significant research has focused on hydrokinetic turbines (HKT), both numerically [3] and experimentally [4]. Among such studies, the experimental work by Bahaj et al. [5,6] is widely regarded as a benchmark for hydrokinetic turbines, owing to its comprehensive experimental characterization and a maximum recorded power coefficient of C_p = 0.46.

While the characteristics of conventional, "freestream" turbines are well understood, only a few studies and industrial applications investigated the potential of diffuser- or duct-augmented HKTs. A duct can benefit the system by (1) facilitating protection from debris and marine life [7], (2) offering additional structural support, and (3) most notably increasing the system's hydrodynamic efficiency.

As a first-order hydrodynamic effect, the presence of a duct increases the mass flow rate through the turbine — and consequently the amount of kinetic energy available for conversion. Adding a duct increases the net power extracted from the same turbine, and can increase the system efficiency for the same maximum frontal area [8] due to better flow conditioning and reduced tip losses. Furthermore, ducted turbines can be optimized to perform more efficiently than freestream turbines under oblique flow conditions [9]. As an additional operational benefit, the duct accelerates the fluid flow at the throat, where the turbine is usually positioned [10,11]. Consequently, the rotational speed can exceed that of a freestream turbine with the same equivalent frontal area because of a smaller turbine diameter and accelerated flow. This increased rotational speed improves generator rotational speed matching, enabling HKTs to operate more efficiently at lower

* Correspondence to: Rm 209, 2600 Draper Dr, Ann Arbor, MI, 48109, USA.
E-mail address: jingsun@umich.edu (J. Sun).
[1] These authors contributed equally to this work.

https://doi.org/10.1016/j.renene.2025.123308
Received 23 September 2024; Received in revised form 17 April 2025; Accepted 27 April 2025
Available online 13 May 2025

Table 1
Summary of experimental studies on hydrokinetic turbines (HKTs). NS indicates values not specified in the respective studies.

Study	Duct design	Comparison baseline	Max C_P	Efficiency gain	Other observations
Scherillo et al. [8]	Diffuser with different pitch	Freestream turbine ($C_P \approx 0.40$)	0.43	+7%	Reduced yaw sensitivity up to 10 deg
Coiro et al. [19]	Optimized diffuser	Freestream turbine	NS	+13%	Highlighted potential of optimization techniques
Shahsavarifard et al. [20]	Two simple diffusers	Freestream turbine (same outlet area)	≤ 0.40	None	No measurable C_P increase, but yaw insensitivity and powertrain simplicity noted
Nunes et al. [21]	Simple duct	Freestream turbine	0.42	+7.5%	Compared based on respective max areas
Roshan et al. [22]	Duct with interior step	Straight duct	NS	Implied	Adding a duct alone does not ensure efficiency gain
Shi et al. [23]	Thin wall diffuser	Freestream turbine ($C_P \approx 0.42$)	0.29	−31%	Raw power output doubled, but normalized C_P dropped
Bahaj et al. [6]	Freestream only	–	0.46	–	Most comprehensive baseline study; not a comparison
This work	Optimized duct (Bahaj rotor)	Freestream turbine (Bahaj geometry)	0.47	+19%	Most efficient ducted design and comprehensive comparative analysis

current speeds. While the structural, environmental, and operational benefits contribute to the overall potential of the system, this study focuses specifically on characterizing the hydrodynamic characteristics of ducted HKTs.

The design of hydrokinetic turbines introduces unique considerations compared to wind turbine design [12], including biofouling effects [13], cavitation [14], and operation at relatively low flow speeds. While the hydroelastic behavior of hydrokinetic turbines shares similarities with the aeroelasticity of wind turbines, the higher fluid density, distinct flow conditions, and added mass effects in water significantly influence the dynamic response and structural interactions [15]. As a result of these differences, hydrokinetic turbines require distinct chord, thickness, and profile distributions compared to wind turbines, as demonstrated by Molland et al. [16] and Bahaj et al. [5].

The addition of a duct to an HKT presents additional challenges due to the complex fluid interactions between the duct and the turbine [11]. Knight et al. [11] demonstrated that if an efficient freestream turbine is placed inside of a duct not purposely designed for the system, the overall turbine performance decreases. They also suggested that a ducted turbine system is typically most efficient at lower blade loading than a freestream turbine. The results from Park et al. [17] further demonstrate that an efficient ducted turbine requires the concurrent design optimization of both the rotor and duct. Building on our previous work in multi-fidelity analysis [18] and concurrent design optimization [17], this study aims to evaluate the performance of a scaled system under realistic operating conditions.

Experimental studies play a critical role in validating both turbine designs and the associated design methodologies. Although a few comprehensive archival experiments exist for ducted turbines (see Table 1), the availability of experimental data specific to ducted hydrokinetic turbines remains limited.

Scherillo et al. [8] compared two diffusers with different duct section pitch angles, based on an analytic design process. It was shown that a diffuser reduced yaw sensitivity up to 10° of flow misalignment. However, their best design showed a C_p increase of just 7% compared to a freestream turbine ($C_p \approx 0.4$ to 0.43), leading to the conclusion that the increase in efficiency was not worth the additional cost and complexity of the system. Higher efficiency improvements ($C_p = +13\%$) where reported for a later experiment on a different configuration by Cairo et al. [19]. The revised diffuser leveraged shape optimization for the duct design, highlighting the potential of this approach for hydrokinetic energy harvesters.

An experimental campaign by Shahsavarifard et al. [20] compared two simple diffuser designs using a small commercial tidal turbine. Neither of the designs showed a measurable increase in the hydrodynamic efficiency ($C_p \leq 0.4$) of the system compared to a freestream turbine with the same diameter as the duct outlet area. Nevertheless, they claimed that the use of a diffuser simplifies the powertrain design and reduces the yaw angle sensitivity. Similarly, Nunes et al. [21] reported efficiency gains within 7.5% ($C_p \approx 0.39$ to 0.42) when comparing the freestream and ducted turbine using their respective maximum area.

Another simple duct design was tested and validated numerically by Roshan et al. [22]. They showed how adding a step on the internal surface of an otherwise straight diffuser can increase its efficiency, further proving that just adding a duct around an existing turbine does not guarantee large efficiency increases. Targeting a different application, a diffuser was specifically optimized to augment the energy harvesting capabilities of an underwater scientific measurement platform by Shi et al. [23]. Their tests showed that their simple thin wall diffuser could double the power output of the system. However, the net power efficiency of the system was reduced when using the duct outlet area to normalize the power coefficient C_p. A more recent experimental validation campaign by Song et al. [24] included a thorough numerical investigation of the effects of duct geometry parameters on the system power output. While the duct-area-based efficiency did not show large improvements compared to the freestream turbine, the camber and pitch angle were shown to vary the power output by almost 50%.

In summary, the body of previous literature on ducted hydrokinetic turbines has predominantly focused on simple duct designs and, with few exceptions, showed relatively small efficiency gains compared to their freestream equivalent. The peak efficiencies of previous ducted turbine studies remain below $C_p \approx 0.45$. Moreover, aside from a few parametric studies, most experimental campaigns have explored limited design spaces when generating power curves and have not examined the impact of varying pitch and flow speed on turbine performance. Notably, the work by Bahaj et al. [5] remains the most comprehensive experimental study on HKTs, conducting a parametric design analysis and achieving a maximum power coefficient of $C_p = 0.46$. As such, their turbine geometry serves as the baseline for our freestream turbine design.

The objective of this work is to quantify the efficiency and power benefits of adding a purposely designed duct to an HKT, and assess its performance at various flow speeds and blade pitch angles. The power and thrust coefficients are calculated based on the maximum frontal area, ensuring a fair comparison of turbine performance. This approach, elaborated by Knight et al. [11], Park et al. [17], and Scherillo et al. [8], has been notably absent in some previous experimental studies. We compare the power coefficient (C_P) and thrust coefficient (C_T) of our ducted system to those of a baseline freestream hydrokinetic turbine

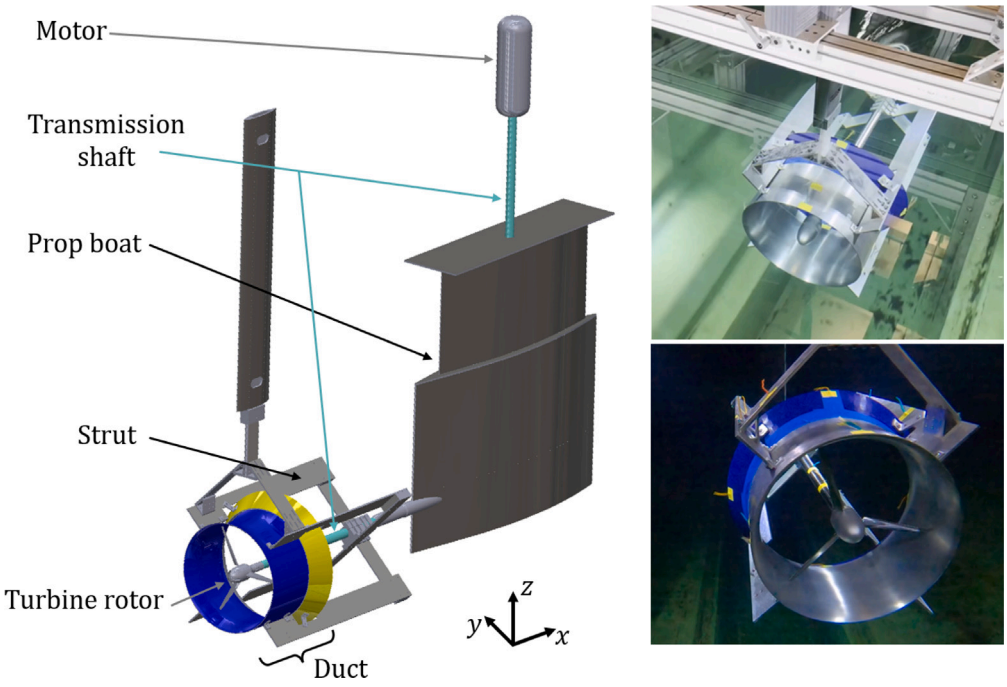

Fig. 1. (Left) CAD of experimental setup, where the flow is along the x-direction; (right) Photographs of submerged turbine.

based on the benchmark geometry by Bahaj et al. [5]. Our study presents a novel experimental database that illustrates the effects of Reynolds number and root pitch on the performance of both freestream and ducted hydrokinetic turbines, using the same rotor design and an optimized duct design.

The experiments were conducted in the University of Michigan's 100 m-long tow tank at various flow and turbine speeds. We used a model scale turbine to fit the existing testing equipment and maintain a blockage [25] of approximately 1%. The tests are performed at flow speeds up to 1.8 m/s for the ducted turbine and 3.08 m/s for the freestream one. The maximum flow speeds are limited by the load limitations of the dynamometer. The measurements are thus performed at a lower Reynolds number than the original benchmark [5]. Nevertheless, we measured a peak $C_P = 0.47$, higher than any efficiency available in literature. For our specific configuration, this corresponds to a 19% efficiency increase compared to our freestream turbine. Moreover, the testing limitations suggest that the turbine design would likely exceed a $C_P = 0.47$ under standard operating conditions.

The remainder of the paper is structured as follows. Section 2 describes the design of the turbine rotor and duct. Section 3 outlines the experimental methodology and summarizes the test campaign. Section 4 presents the experimental results, including post-processing details in Section 4.1, and discussions on the freestream (Section 4.2) and ducted turbine (Section 4.3) results. Section 4.2 compares the experimental results of this study with those in [5,6], highlighting key differences in operational conditions and test item. Section 4.3 examines the performance trends observed in ducted turbines across (1) various pitch angles, (2) different flow speeds, and (3) a comparison of ducted versus freestream turbines. Finally, Section 5 concludes the paper and suggests directions for future research.

2. Test component specifications

The ducted turbine concept tested in this experimental campaign is a combination of legacy design and specially developed components. A CAD model of the full assembly is shown in Fig. 1, next to two pictures of the test items in the Marine Hydrodynamics Lab (MHL) tank. The turbine geometry is based on Bahaj et al. [5]. The duct shape was optimized with the same approach developed by Park et al. [17]. The duct was originally designed using numerical tools that idealized the duct as a thin-walled axisymmetric structure shrouding the turbine.

The duct shape was optimized together with the turbine geometry [17], so the choice of using the benchmark turbine geometry from Bahaj et al. [5] likely reduces the maximum efficiency of the ducted system we tested. The idealized structure in the numerical tool required several modifications to be manufactured and outfitted for experimental measurement. The modifications are a deliberate step from simulation-based convenience toward real-world deployment. The necessary modifications for the assembly integration are discussed later in this section.

We manufactured a single turbine and duct for this testing campaign to fit testing schedule and manufacturing cost constraints. A more extensive study investigating blade chord and twist profiles, tip gaps, along with duct sectional shapes, would be academically relevant, but it extends well beyond the scope of the present work.

2.1. Mechanical assembly

The turbine model is mounted to an apparatus known as a "propeller boat" (see Fig. 1), which consists of a forward-oriented horizontal shaft that protrudes from a foil-shaped strut that houses the thrust and torque dynamometer. An electric servo motor is mounted above a vertically oriented drive shaft that is connected to the horizontal shaft by a 90° gearbox.

A dynamometer (HR Wallingford model R25-01) is connected in line with the turbine shaft. It has a maximum torque of 10 N-m and a maximum thrust of 250 N. The dynamometer has a low nonlinearity error of 0.1% and a measurement sensitivity of 0.16 mV/V. The details of the electrical equipment are provided in Section 3.

The duct is mounted coaxially on the shaft through four struts and connected to the shaft itself aft of the duct outlet, as shown in Fig. 1. The struts hold in place both the metallic duct body and a 3D-printed outlet, further described in Section 2.2. To mitigate potential rig oscillations, a fin is mounted above the duct, close to the inlet. This fin is not joined with the rest of the duct and the struts to allow in the negative z direction and prevent duct misalignment during installation.

Alignment accuracy is essential for the safety and integrity of the structure. Moreover, the turbine performance is highly sensitive to the

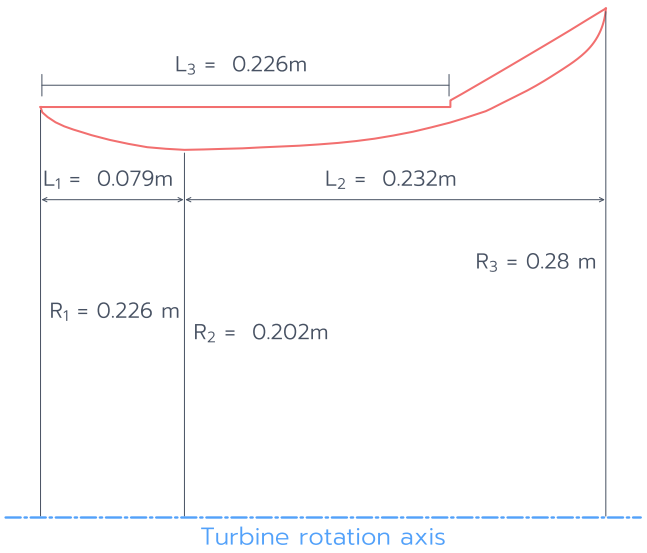

Fig. 2. CAD model of the experimental duct showing the radii at the inlet (R_1), throat (R_2), and outlet (R_3), and the axial distance between the duct inlet and throat (L_1), throat and outlet (L_2), and inlet and brim (L_3). All dimensions are in meters.

tip gap. The duct axial alignment is set so that the turbine is installed at the duct's throat (i.e., the position with the smallest cross-sectional area).

2.2. Duct design

The duct geometry is derived from an intermediate design presented in Park et al. [17], which assumed a thin-walled duct. We used this duct profile as the internal surface of the experimental duct. The duct is split into two sections, as shown in Fig. 2.

The front (inlet) section is lathed from an aluminum block with a cylindrical outer surface. The outlet section of the duct is made of ABS (acrylonitrile butadiene styrene) through 3-D printing. The 3-D printing allowed for more design and installation flexibility during the experiment preparation. We decided on a truncated cone outer shape to minimize flow separation and separation-induced vibrations. This 3-D-printed brim is installed in position through the same strut that supports the rest of the duct, discussed in the next section.

2.3. Turbine design

The turbine analyzed in this work is a three-bladed turbine. The blade design has the same twist, normalized chord, and thickness profile as the blades of Bahaj et al. [5]. However, our turbine is one-half the size of the Bahaj one, resulting in a rotor diameter of 0.4 m. The turbine blades are made from stainless steel and are attached to an adjustable pitch assembly that allows for 5° increments in turbine blade pitch. In our current study, we consider pitch angles of 22°, 27°, and 32° for both the freestream and ducted turbines. These pitch values account for a $\approx 2° \pm 0.5°$ manufacturing and assembly offset measured on the turbine and hub assembly. For the ducted turbine, the tip gap was minimized to reduce tip losses and enhance performance. A 2 mm tip gap was achieved, constrained by manufacturing tolerances and assembly limitations. Notably, our system, with a tip gap ratio of 1% (tip gap to turbine radius), demonstrated significantly greater performance improvements – up to 13% – compared to previous studies with similar tip gap ratios (ranging from 1.5% [20] to 5.6% [21]). Throughout our experiments, the tip gap remained constant, as a single blade and duct were fabricated. A more comprehensive investigation into the impact of tip losses on ducted turbine performance is left for future endeavors.

The turbine is attached to the propeller boat shaft, which is driven by the tow tank carriage. The propeller boat shaft is connected to the motor to provide the target rotation rate, ω, for each tip speed ratio, λ, and carriage speed, v, as discussed in Section 3. The tip-speed ratio λ is defined as

$$\lambda = \frac{\omega R}{v}, \tag{1}$$

where $R = 0.2$ m is the turbine radius, ω the blade rotation speed, and v the carriage tow speed, equivalent to the apparent flow speed experienced by the HKT.

3. Experimental methodology

3.1. Tow testing setup

The experimental study was conducted at the Aaron Friedman Marine Hydrodynamics Laboratory at the University of Michigan, which features a 100 m long towing tank. The turbine hub was immersed to a depth of approximately 1 m. The tow tank is 6.5 m wide and 3.5 m deep, resulting in a blockage of 1.08% relative to the turbine duct's maximum area. The entire mechanical assembly is lowered in the water and clamped to the carriage while testing. The tow speed of the carriage is measured with encoders on the rail with an error of ± 0.02 m/s.

3.2. Instrumentation

The electrical setup includes a 3 kW Kollmorgen AKM54L-ANC2C-00 motor that acts as a generator, which is connected to a three-blade turbine rotor via shaft transmission. As shown in Fig. 1, the rotating shaft (teal color) is redirected orthogonally inside a foil-shaped waterproof housing (fin). This configuration allows the use of a non-submersible motor. The motor and dynamometer are connected to an NI data acquisition system (NI cRio 9045) with real-time control software implemented in Labview. A PI controller is used to close the loop on turbine speed, which is measured with an internal encoder. The energy generated by the motor is dissipated as heat through a resistive load.

3.3. Testing campaign summary

The campaign's goal was to characterize the ducted turbine's performance and quantify the efficiency and power increase compared to the freestream turbine. To achieve this goal, we tested the two turbine configurations over a range of blade pitch settings, inflow velocities, and rotation rates — all the turbine parameters that do not require additional component manufacturing. The testing envelope was bounded by the measuring instrumentation load limits in both torque (at low rotation speeds) and thrust (at high rotation speeds). Only minor rig oscillations were observed at high speeds (v) and tip-speed ratios (λ). These speeds were not high enough to jeopardize the structural integrity of the setup but can be observed as larger signal oscillations in the recorded data.

Given these considerations, we measured the torque and thrust of the ducted turbine for tip-speed ratios between 4 and 8, and flow speeds ranging from 1.4 m/s to 1.8 m/s. A few test runs reached flow speeds as high as 2.0 m/s. The freestream turbine was tested up to 3.08 m/s to match the Reynolds number of one of the runs from Bahaj et al. [5]. The testing parameters are listed in Table 2. We ran λ sweeps at a minimum resolution of 0.5, with higher measurement density (up to 0.06) in the proximity of the C_P peaks. The blade pitch was set at 22°, 27°, and 32° for the ducted and freestream tests. A total of more than 300 individual data points were collected. The test results are summarized and discussed in Section 4.

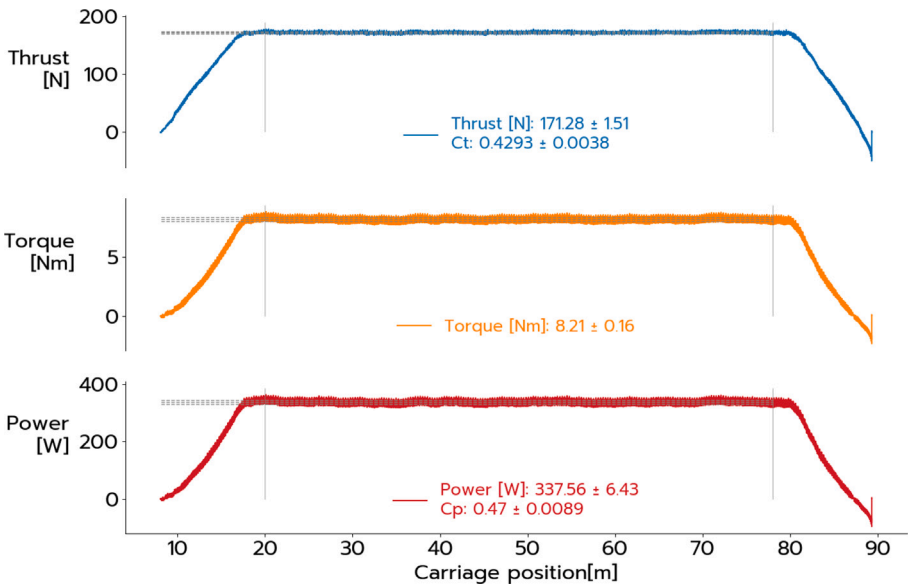

Fig. 3. Sample time-series (top to bottom): Thrust, torque, and power versus carriage position for a v = 1.8 m/s run with the ducted turbine.

Table 2
Testing parameters.

Speed	1.4 m/s–1.8 m/s (+ 3.08 m/s)
λ	4–8
Blade pitch settings	22°, 27°, 32°
Turbine types	Ducted, Freestream

4. Results

This section describes the data post-processing and presents the key findings of our experimental campaign. The measured loads are reported in terms of power coefficient (C_P) and thrust coefficient (C_T). These coefficients were computed as follows:

$$C_P = \frac{\tau\omega}{0.5\rho A v^3}, \qquad C_T = \frac{T}{0.5\rho A v^2}, \tag{2}$$

where τ is the measured torque, ω is the rotor speed, ρ is the water density, A is the maximum area of the HKT (rotor swept area for freestream turbine and outlet area for the ducted turbine), T is the measured thrust, and v is the flow (tow) speed. We use the swept rotor area to normalize the loads for the freestream turbine. Consistent with the definition used by Park et al. [17], the ducted turbine loads are normalized with respect to the duct outlet, which corresponds to the maximum cross-sectional area of the system. The reference diameters are $D_{\text{freestream}} = 0.4$ m and $D_{\text{ducted}} = 0.56$ m, respectively.

For each speed and blade pitch angle, we test a range of λ and compare the C_P and C_T curves over the measured operating range. The C_P provides a direct indication of the power that the turbine can extract from the water flow and, consequently, the system's efficiency. Lower axial loads (indicated by C_T) indirectly affect the levelized cost of energy due to the lighter structure needed to support the turbine in operation.

Section 4.1 summarizes the data processing we used in this experimental campaign. In Section 4.2, we characterize our freestream HKT and benchmark it against Bahaj et al. [5], quantifying the performance losses and suggesting potential modifications to minimize this performance gap. In Section 4.3, we analyze the results of the ducted turbine and compare its performance to the freestream one. Given the strong Reynolds number effects we observed on the freestream HKT, we expect the ducted turbine to have higher performance at full-scale and nominal inflow conditions.

4.1. Post-processing details

Thrust and torque measurements at the dynamometer, along with motor speed measurements, are used to compute the HKT's hydrodynamic coefficients. A time-series dataset is associated with each tow run in the experimental study, during which the flow speed was held constant. A sample time series is shown in Fig. 3, plotting the torque and thrust measurements, as well as the computed power measurements. Filtering and normal fitting are used to obtain the mean value of each sensor measurement, which is eventually used to generate the C_P and C_T curves. Based on the measurement noise observed and standard error propagation principles [26], the net error in C_P was computed to be less than $C_P \pm 0.01$.

4.2. Freestream turbine performance

The turbine is first examined without a duct (i.e., in freestream conditions) to compare to the experiments of Bahaj et al. [5]. Fig. 4 depicts the test setup for the freestream turbine, fully assembled and deployed, after the removal of the surrounding duct. The turbine tested in the current work is examined at three different mounting angles (22°, 27°, and 32°), while the Bahaj's experiment examined different turbine at blade pitches (20°, 25°, 27°, and 30°).

As mentioned in Section 3.3, the turbine tested in the current work is half the scale of the turbine tested by Bahaj et al. [5]. Due to limitations of available dynamometry, matching the Reynolds number of the Bahaj et al. [5] experiments by doubling the flow speed was not feasible in this study. Furthermore, due to the smaller scale used in the current work, manufacturing imperfections and surface roughness of the turbine would be magnified relative to the original Bahaj's turbine.

Fig. 5 shows the pitch sensitivity of Bahaj et al. [5] and our own tested turbine at different blade pitch settings. The lowest pitch settings have the highest C_P values in both experiments. While a pitch variation of 5° generally leads to changes in C_P between 0.05 and 0.1, both campaigns registered minimal pitch sensitivity at certain mounting angles: 22° and 27° for the current work, and 27° and 30° for Bahaj et al. [5].

The highest $C_P = 0.46$ from Bahaj et al. [5] outperforms the $C_P = 0.39$ from the current experiments. This is likely due to Reynolds number effects and manufacturing tolerances mentioned above. The freestream setting with the highest C_P in our campaign (22°) has a lower C_T than the 20° results from Bahaj et al. [5] because the turbine blades are set at a higher pitch angle. The same effect is

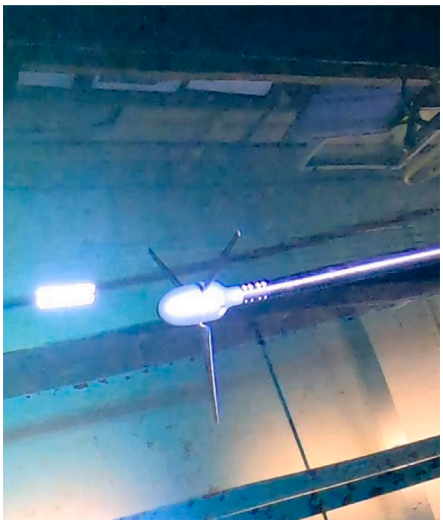

Fig. 4. Submerged freestream turbine.

observed between our freestream turbine at 32° and Bahaj et al. [5] at 30°. Moreover, at the 32° blade pitch, the Reynolds number effect is observed for carriage velocities of 1.8 m/s and 3.08 m/s.

With increasing Reynolds number, both the C_P and C_T increase. At the nominal testing range Re ≈ 100 000, the turbine blades fully operate in the boundary layer transitional regime. The blade manufacturing rugosity is also likely to affect transition. Increasing the flow speed, the blades generate loads more efficiently because the boundary layer transition occurs closer to the leading edge, reducing the blade drag.

A similar Reynolds number effect is seen in Fig. 6, where we compare the two turbines at the same 27° blade pitch angle. The load coefficients on our turbine increase with the flow speed. The C_T between the current experiments and Bahaj et al. [5] experiments are in closer agreement than C_P. The peak C_T is higher in the Bahaj et al. [6] experiments than the current results and also occurs at a lower λ than the current experiments. The maximum C_P in the Bahaj's experiments [5] is lower and occurs at a lower λ than the current experiments for the 27° blade pitch angle. These deviations could be due to differences in blade manufacturing tolerance, such as surface roughness, as well as Reynolds number effects.

Finally, Fig. 7 shows the sensitivity to inflow velocity for both our and Bahaj et al. [5] experiments at the respective highest C_P settings. Despite the measurement scatter at the lowest speed, Bahaj's results overlap consistently despite the 0.27 m/s velocity difference between the two measurements, which were also measured in two different test settings [6]. A 0.4 m/s difference at the same pitch angle for our turbine leads to a difference of at least $C_P = 0.03$ for $\lambda > 5.5$ and up to $C_P = 0.1$ at $\lambda = 4.5$, where the Reynolds effects are higher due to the lower rotation speed.

4.3. Ducted turbine performance

We present three sets of comparisons between different blade pitches and flow speeds. The performance of the ducted system is investigated at different blade pitch angles (Section 4.3.1) and inflow velocity (Section 4.3.2). The comparison between ducted and freestream turbines is shown in Section 4.3.3. Peak and average C_P around the optimal λ are reported in Table 3, together with the corresponding C_T. The average $C_{P_{avg}}$ in Table 3 is obtained by averaging the C_P between $\lambda = 4.5$ and $\lambda = 5.5$. In real-time operations, the controller might struggle to exactly match the λ for such sharp power curve around the $C_{P_{max}}$. Assessing the performance of the turbine over a range of λ close to the optimal rotation rate provides a fairer comparison for actual operational C_P.

4.3.1. Blade pitch variation

We first characterize the ducted turbine for different blade pitch settings to identify the blade mounting angle with the best C_P and C_T curves. We compare the power curves for the 32°, 27°, and 22° blade pitch setting at a fixed carriage speed $v = 1.4$ m/s in Fig. 8. The ducted turbine provides high power efficiency over a range of blade pitch settings.

In contrast to the freestream case, the lowest pitch angle is the worst performing for the ducted setup. A low root pitch corresponds to higher hydrodynamic loading on the blade. These higher loads reduce the mass flow rate through the duct. A lower mass flow rate reduces the total available kinetic energy flowing through the duct and commensurately reduces the power extracted by the turbine. Our results suggest that the ducted turbine should operate at a lower loading, and namely higher pitch, than the freestream turbine equivalent.

With a blade pitch setting of 22°, the maximum C_P is just above 0.39 and decreases sharply at suboptimal λ. The other two pitch settings have closely matched power curves. We measured a peak efficiency of $C_P = 0.458$ at $\lambda = 4.5$ for the 32° pitch at the 1.4 m/s flow speed. While the peak $C_{P_{max}}$ for the 27° pitch setting is lower within measurement error ($C_P = 0.456$), its C_P curve is less sharp, and the C_P is 0.005 to 0.02 higher for $\lambda > 5$. This makes it more suitable for real-world applications with peak-tracking turbine controllers. At the same time, the 32° configuration has a higher pitch angle and thus has a lower thrust. As shown later in this section, this configuration has shown the highest overall C_P at higher flow speeds. This illustrates that the ducted turbine performs better with a higher blade pitch angle at lower C_T loading than a freestream turbine.

As shown in Section 4.2, a blade pitch change of 5° is expected to show larger performance differences than what is shown in Fig. 8. We suspect that the two pitch configurations are almost equally distanced from an optimal setting between 27° and 32°. This motivates further analyses conducted on a blade with a tailored twist distribution that can be installed at the effective optimal pitch.

4.3.2. Flow speed variation

As for the freestream turbine (Section 4.2), the carriage flow speed has a measurable effect on the system efficiency at this experimental scale and flow regime. The sub-scale turbine is operating at a critical Reynolds number (10^5), where boundary layer transition effects dominate the flow behavior on the blade and the duct. Increasing the testing speed takes the turbine beyond this unstable regime and closer to real-world operating conditions. Moreover, the blade surface has not been polished as done by Bahaj et al. [5], who performed cavitation studies and thus needed a very smooth surface. Our model's rougher blade surface increases the probability of triggering the boundary layer laminar–turbulent transition at lower speeds.

Fig. 9 compares four power curves for equally-spaced velocities between 1.8 m/s and 1.4 m/s. The lowest speed of the set shows a lower C_P peak and consistently worse performance for $\lambda > 5$ at a comparable thrust coefficient C_T. As the speed is increased up to 1.8 m/s, the power and thrust coefficient curves match more closely. The C_P nevertheless keeps increasing with increasing speed. We measured a peak $C_P = 0.47$ at $\lambda = 4.57$ and $v = 1.8$ m/s. The average $C_P = 0.454$ between $\lambda = 4.5$ and $\lambda = 5.5$ is also the highest among all tested speeds and pitch settings, as shown in Table 3.

This power coefficient ($C_P = 0.47$) is the highest measured efficiency for a hydrokinetic turbine system reported in the literature. This value is higher than the original benchmark from Bahaj et al. [5] by at least $C_P = 0.01$ (1% higher system efficiency) on a sub-scale turbine that operates at a lower and less favorable Reynolds number. Further testing with updated sensors that can withstand higher loads would enable even more realistic testing conditions and would likely show further efficiency improvements. Moreover, the turbine we used was not optimized when coupled with the duct. The design approach of Park et al. [17], which simultaneously optimizes the blade and duct geometries, is likely to increase the efficiency further.

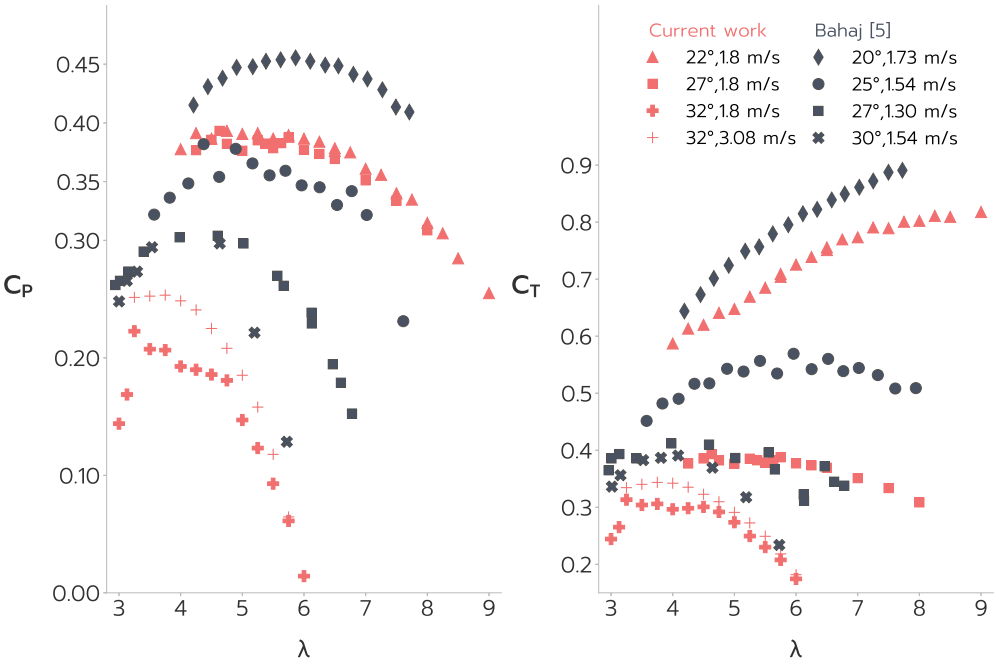

Fig. 5. Comparison between Bahaj [5] (black symbols) and the freestream turbine (red symbols) used in this work.

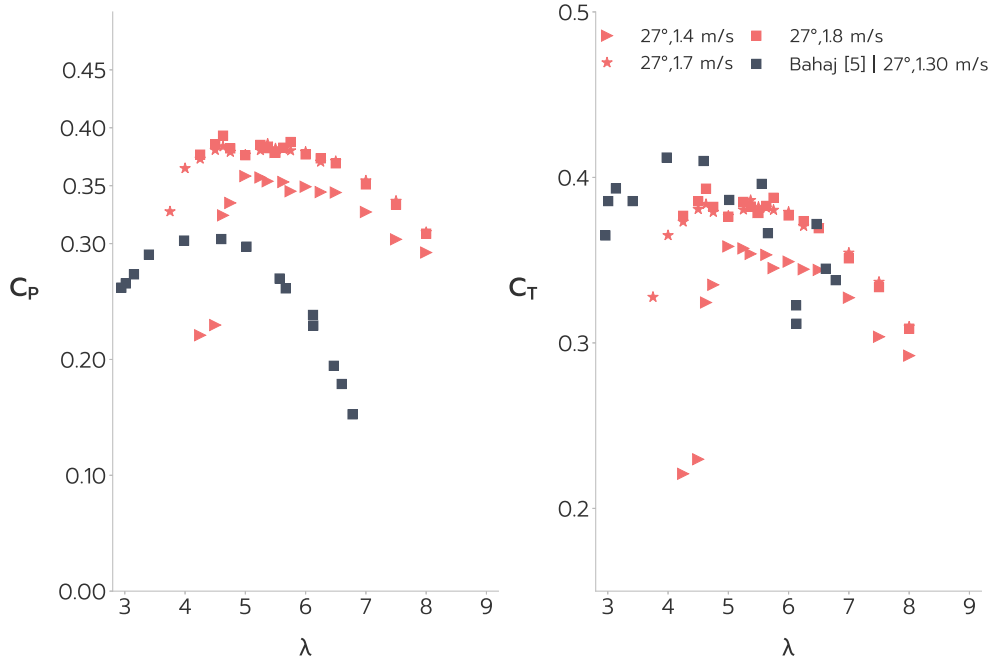

Fig. 6. Comparison between Bahaj [5] and the freestream turbine used in this work at the matching pitch setting of 27°.

4.3.3. Comparison between freestream and ducted turbines

To further emphasize the efficiency gain due to the duct, we compare the best-performing freestream pitch setting (22°) against the best-performing ducted pitch setting (32°) in Fig. 10. Adding the duct increases the C_P from 0.39 to 0.47, a 19% increase compared to the baseline freestream turbine.

We suspect that this increase is due to a combination of increased mass flow rate through the turbine and the higher Reynolds number, both enabled by the duct shrouding the turbine. This increase is specific to the turbine configuration and testing conditions. There is no direct way to estimate the direct impact of a duct for different turbines operating in different conditions. However, Park et al. [17] and previous literature presented in Section 1 show that a bad duct design can be detrimental to overall performance. At the same time, co-designed blade and turbines enable higher performance gains. Aside the Reynolds effects we investigated (Fig. 7), different flow turbulence levels would also likely affect the peak turbine performance. However, a well-designed duct would improve the flow conditioning and likely make the turbine less sensitive to flow velocity fluctuations [17].

The power curve profile would also likely change based on different operating conditions. For our tested configuration, the efficiency decreases almost linearly with RPM around the peak but remains consistently higher than the freestream case over the tested operating envelope. Because the best pitch of the ducted turbine (32°) has a higher pitch angle than the freestream case, the thrust coefficient is almost 30% lower than for the freestream case.

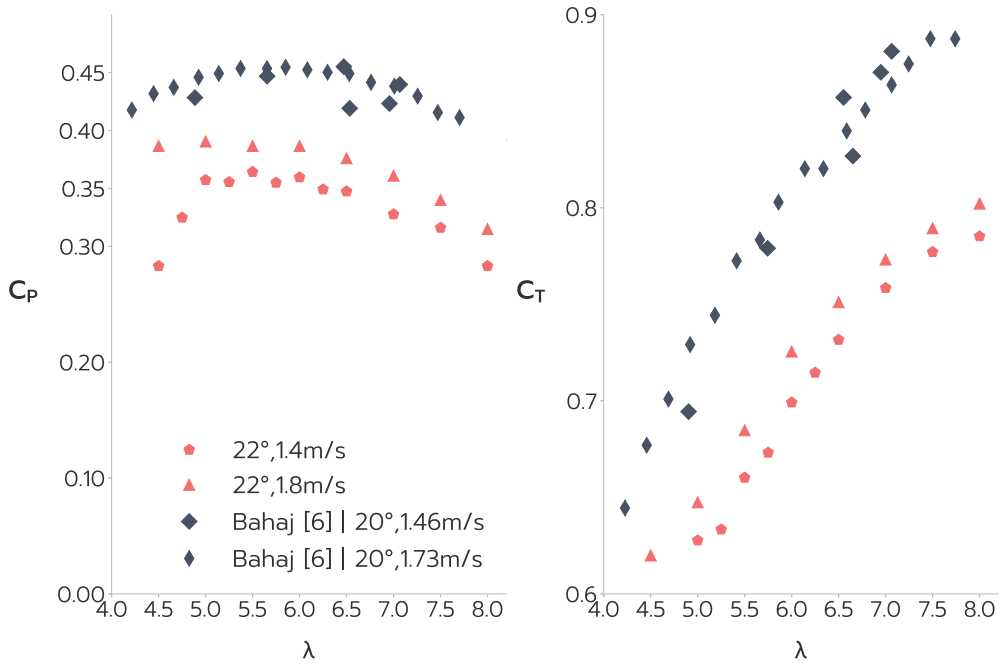

Fig. 7. Velocity sensitivity of the Bahaj [5] turbine at 20° and our freestream turbine at 22°.

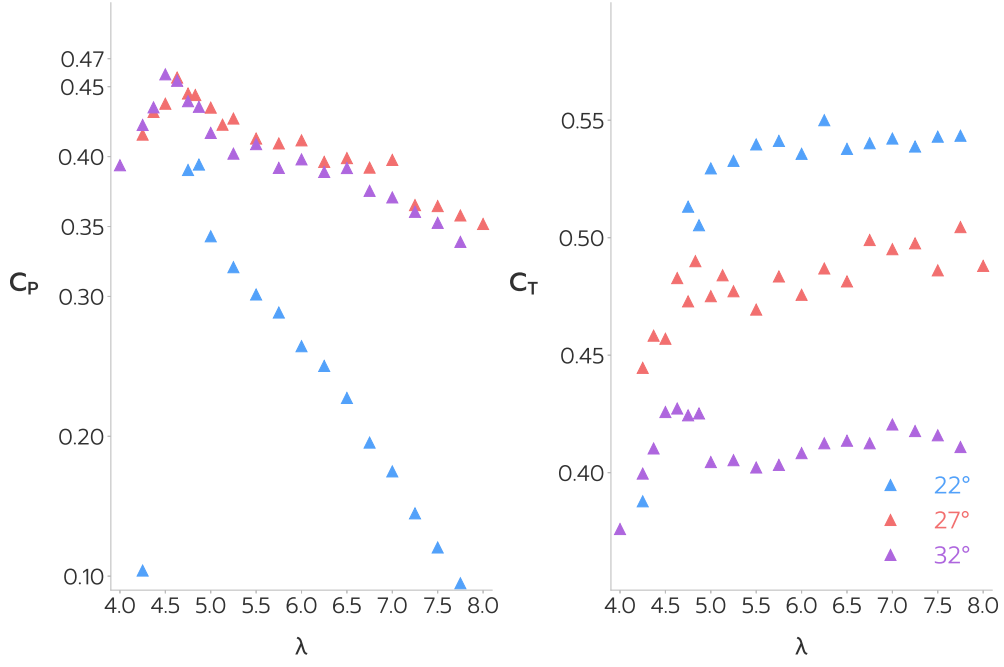

Fig. 8. Blade pitch sensitivity of the ducted turbine at v = 1.4 m/s.

Table 3
Results summary for each C_P and C_T curve for the ducted turbine and the best freestream one. We report the highest measured C_P and the C_T at the same condition and averaged values of both C_P and C_T for $\lambda = 4.5$ and $\lambda = 5.5$.

Turbine type	Pitch [°]	Speed [m/s]	$C_{P_{max}}$	C_T @ $C_{P_{max}}$	$C_{P_{avg}}$	$C_{T_{avg}}$	Fig(s).
Freestream	22	1.8	0.394	0.653	0.39	0.653	10
Ducted	32	1.8	0.47	0.429	0.454	0.426	9, 10
Ducted	32	1.4	0.46	0.426	0.431	0.416	8, 9
Ducted	27	1.4	0.456	0.483	0.435	0.476	8
Ducted	22	1.4	0.394	0.505	0.35	0.524	8
Ducted	32	1.7	0.461	0.428	0.445	0.422	9
Ducted	32	1.6	0.469	0.429	0.451	0.426	9

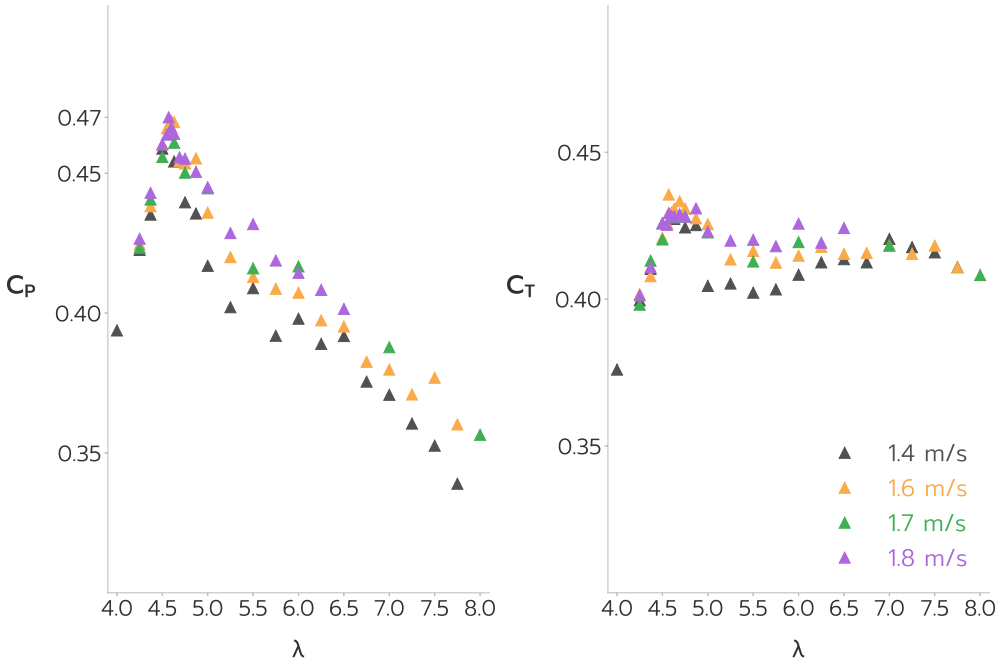

Fig. 9. Flow speed sensitivity of the ducted turbine at blade pitch setting of 32°.

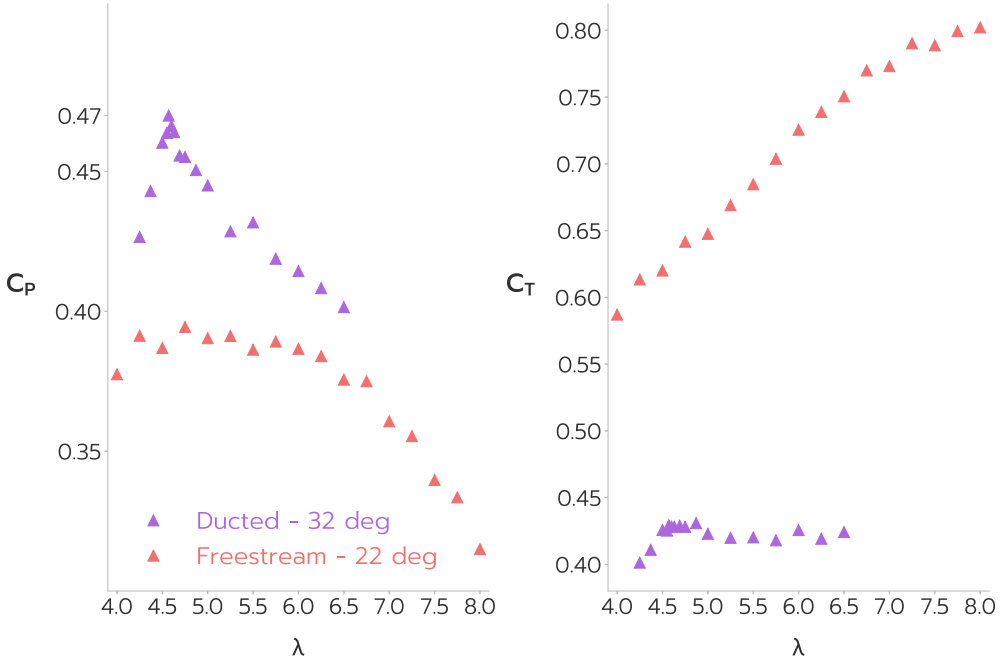

Fig. 10. Comparison of best ducted and freestream turbines at $v = 1.8$ m/s.

5. Conclusion

In this paper, we present the result of an experimental campaign on a ducted hydrokinetic turbine conducted at the University of Michigan's Marine Hydrodynamics Laboratory. We coupled a sub-scale turbine rotor based on Bahaj's geometry with an optimized duct from a parallel research effort. The duct was manufactured using different techniques and fit in a preexisting test rig, which we used to measure torque and thrust outputs at a prescribed inflow speed and rotation rate.

The freestream HKT performance was first characterized and compared to the Bahaj's experimental campaign to quantify the effect of Reynolds number and manufacturing details. We then measured the performance improvements obtained through an in-house-designed duct and characterized the system performance over a range of blade pitch settings and flow regimes. Our duct design increases the power by up to 19% compared to the freestream turbine. We reliably measured a peak power coefficient of 0.47, surpassing the Bahaj benchmark with a smaller and less refined turbine.

The ducted turbine power peak is sharper than the characteristic power curve of a freestream turbine. Nevertheless, we observed a large operational range in terms of blade pitch setting, with similar power outputs within ±2.5° from the optimal setting. Moreover, the ducted turbine is more efficient than the freestream turbine at higher blade pitch angles and lower C_T loading. Our system sensitivity to inflow velocity is higher than Bahaj's freestream turbine. This is likely because

the scale effects put the turbine within an unfavorable transitional Reynolds number regime.

This campaign opens the door to further numerical and experimental studies. Higher efficiencies are likely to be obtained on the same design by extending the flow speed testing range, increasing the turbine and duct scale, and ensuring higher blade manufacturing quality and surface polishing. Using updated and co-optimized blade and duct geometries would further enhance the system performance, according to recently published numerical optimization studies [17]. Given the influence of the duct external geometry on the turbine performance, improved packaging and duct external geometry refinements could improve the ducted turbine further. As the turbine is scaled up, it is also expected that the performance will improve due to Reynolds effects. This study has demonstrated a strong Reynolds number dependence for the low-Reynolds number conditions at which the test is carried out. Furthermore, a revised optimization process that accounts for off-design conditions, such as misaligned flow, ambient turbulence, and effects of waves, would increase the ducted HKT energy yield in real-world operating conditions.

Overall, this study further validates the concept of a ducted turbine as a high-efficiency renewable energy converter for tidal and riverine applications. Future research should address robustness, operability, and maintainability. An upscaled model designed with further electromechanical and environmental impact mitigation considerations could be deployed in real-world scenarios to improve performance and reduce the cost of energy and fossil-fuel reliance for isolated communities and industrial installations.

CRediT authorship contribution statement

Kartik Naik: Supervision, Software, Resources, Project administration, Methodology, Investigation, Funding acquisition, Formal analysis, Data curation, Conceptualization. **Marco Mangano:** Writing – review & editing, Writing – original draft, Visualization, Validation, Methodology, Formal analysis, Data curation, Conceptualization. **Bradford G. Knight:** Writing – review & editing, Writing – original draft, Validation, Methodology, Investigation, Formal analysis, Data curation, Conceptualization. **Sabet Seraj:** Writing – review & editing, Visualization, Methodology, Investigation, Formal analysis, Data curation, Conceptualization. **Yingqian Liao:** Writing – review & editing, Formal analysis, Data curation, Conceptualization. **Jeongbin Park:** Resources, Data curation, Conceptualization. **Yulin Pan:** Writing – review & editing, Supervision, Methodology, Investigation, Funding acquisition. **Joaquim R.R.A. Martins:** Writing – review & editing, Supervision, Resources, Funding acquisition. **Kevin J. Maki:** Writing – review & editing, Supervision, Project administration, Funding acquisition. **Jing Sun:** Writing – review & editing, Supervision, Project administration, Funding acquisition, Conceptualization.

Declaration of competing interest

The authors declare that they have no known competing financial interests or personal relationships that could have appeared to influence the work reported in this paper.

Acknowledgments

This work was supported by the US Department of Energy under the award “RAFT: Reconfigurable Array of High-Efficiency Ducted Turbines for Hydrokinetic Energy Harvesting” (Award No. DE-AR0001438). The authors thank DOE ARPA-E Submarine Hydrokinetic And Riverine Kilomegawatt Systems (SHARKS) Program led by Mario Garcia-Sanz. We owe a special thanks to the entire SHARKS Team for their support. The authors would like to gratefully acknowledge the staff at the Aaron Friedman Marine Hydrodynamics Laboratory for their expert help in designing and performing the experiments on our design.

References

[1] L. Kilcher, M. Fogarty, M. Lawson, Marine energy in the United States: An overview of opportunities, 2021.
[2] A.R. Winslow, Urban wind generation: comparing horizontal and vertical axis wind turbines at clark university in worcester, massachusetts, 2017.
[3] L. Lago, F. Ponta, L. Chen, Advances and trends in hydrokinetic turbine systems, Energy Sustain. Dev. 14 (4) (2010) 287–296.
[4] P.M. Jamieson, Beating Betz: energy extraction limits in a constrained flow field, 2009.
[5] A. Bahaj, A. Molland, J. Chaplin, W. Batten, Power and thrust measurements of marine current turbines under various hydrodynamic flow conditions in a cavitation tunnel and a towing tank, Renew. Energy 32 (3) (2007) 407–426.
[6] A. Bahaj, W. Batten, G. McCann, Experimental verifications of numerical predictions for the hydrodynamic performance of horizontal axis marine current turbines, Renew. Energy 32 (15) (2007) 2479–2490.
[7] E. Asok, R.-Q. Wang, Environmental co-design: Fish-blade collision model for hydrokinetic turbines, 2025, [Online]. Available: https://arxiv.org/abs/2502.15161.
[8] F. Scherillo, U. Maisto, G. Troise, D. Coiro, S. Miranda, Numerical and experimental analysis of a shrouded hydroturbine, in: 2011 International Conference on Clean Electrical Power, ICCEP, IEEE, 2011, pp. 216–222.
[9] M. Rivarolo, A. Freda, A. Traverso, Test campaign and application of a small-scale ducted wind turbine with analysis of yaw angle influence, Appl. Energy 279 (2020) 115850, [Online]. Available: https://www.sciencedirect.com/science/article/pii/S0306261920313271.
[10] M.J. Werle, W.M. Presz Jr., Ducted wind/water turbines and propellers revisited, J. Propuls. Power 24 (5) (2008) 1146–1150.
[11] B. Knight, R. Freda, Y.L. Young, K. Maki, Coupling numerical methods and analytical models for ducted turbines to evaluate designs, J. Mar. Sci. Eng. 6 (2) (2018) 43.
[12] T. Ashuri, J.R. Martins, M.B. Zaaijer, G.A. van Kuik, G.J. van Bussel, Aeroservoelastic design definition of a 20 MW common research wind turbine model, Wind. Energy 19 (11) (2016) 2071–2087.
[13] H. Rashid, M. Benbouzid, H. Titah-Benbouzid, Y. Amirat, A. Mamoune, Tidal stream turbine biofouling detection and estimation: A review-based roadmap, J. Mar. Sci. Eng. 11 (5) (2023) [Online]. Available: https://www.mdpi.com/2077-1312/11/5/908.
[14] H.P. Picanço, A. Kleber Ferreira de Lima, D.A.T. Dias do Rio Vaz, E.F. Lins, J.R. Pinheiro Vaz, Cavitation inception on hydrokinetic turbine blades shrouded by diffuser, Sustainability 14 (12) (2022) [Online]. Available: https://www.mdpi.com/2071-1050/14/12/7067.
[15] N. Kolekar, A. Banerjee, A coupled hydro-structural design optimization for hydrokinetic turbines, J. Renew. Sustain. Energy 5 (5) (2013) 053146.
[16] A.F. Molland, A.S. Bahaj, J.R. Chaplin, W.M.J. Batten, Measurements and predictions of forces, pressures and cavitation on 2-d sections suitable for marine current turbines, Proc. Inst. Mech. Eng. Part M: J. Eng. Marit. Environ. 218 (2) (2004) 127–138.
[17] J. Park, B.G. Knight, Y. Liao, M. Mangano, B. Pacini, K.J. Maki, J.R. Martins, J. Sun, Y. Pan, CFD-based design optimization of ducted hydrokinetic turbines, Sci. Rep. 13 (1) (2023) 17968.
[18] B.G. and Knight, J. Park, Y. Liao, M. Mangano, Y. Pan, J.R. Martins, K.J. Maki, Multifidelity Cfd Analysis for Ducted Hydrokinetic Turbine Design, Available At SSRN, Preprint.
[19] D.P. Coiro, E. Daniele, P. Della Vecchia, Diffuser shape optimization for GEM, a tethered system based on two horizontal axis hydro turbines, Int. J. Mar. Energy 13 (2016) 169–179.
[20] M. Shahsavarifard, E.L. Bibeau, V. Chatoorgoon, Effect of shroud on the performance of horizontal axis hydrokinetic turbines, Ocean Eng. 96 (2015) 215–225.
[21] M.M. Nunes, R.C. Mendes, T.F. Oliveira, A.C.B. Junior, An experimental study on the diffuser-enhanced propeller hydrokinetic turbines, Renew. Energy 133 (2019) 840–848.
[22] S.Z. Roshan, S. Alimirzazadeh, M. Rad, RANS simulations of the stepped duct effect on the performance of ducted wind turbine, J. Wind Eng. Ind. Aerodyn. 145 (2015) 270–279.
[23] W. Shi, D. Wang, M. Atlar, B. Guo, K.-c. Seo, Optimal design of a thin-wall diffuser for performance improvement of a tidal energy system for an AUV, Ocean Eng. 108 (2015) 1–9.
[24] K. Song, W.-Q. Wang, Y. Yan, Numerical and experimental analysis of a diffuser-augmented micro-hydro turbine, Ocean Eng. 171 (2019) 590–602.
[25] R. He, H. Sun, X. Gao, H. Yang, Wind tunnel tests for wind turbines: A state-of-the-art review, Renew. Sustain. Energy Rev. 166 (2022) 112675.
[26] J. Kirchner, Data Analysis Toolkit# 5: Uncertainty Analysis and Error Propagation, University of California Berkeley Seismological Laboratory, 2001, Available Online At: http://seismo.berkeley.edu~{}kirchner/eps_120/Toolkits/Toolkit_05.pdf.